RESEARCH ARTICLE | JANUARY 15 2019

A high-performance bending magnet beamline (BL02B) at the SSRF

Xiangyu Meng; Zhi Guo; Yong Wang; Fangyuan Zhu; Hui Zhang; Nian Zhang; Renzhong Tai

AIP Conf. Proc. 2054, 030011 (2019)
https://doi.org/10.1063/1.5084574

A High-performance Bending Magnet Beamline (BL02B) at the SSRF

Xiangyu Meng[1], Zhi Guo[1, a)], Yong Wang[1, b)] Fangyuan Zhu, Hui Zhang, Nian Zhang and Renzhong Tai[1, c)]

[1]*Shanghai Institute of Applied Physics, Chinese Academy of Sciences, Zhangheng Road 239, Pudong District, Shanghai, 201800, China*

[a)]Corresponding author: guozhi@sinap.ac.cn
[b)]wangyong@sinap.ac.cn
[c)]tairenzhong@sinap.ac.cn

Abstract. The BL02B beamline at the Shanghai Synchrotron Radiation Facility (SSRF) has a high energy resolution and high photon flux. It is now operational for ambient pressure photoelectron spectroscopy (APPES) and photon-in/photon-out spectroscopy (PIPOS) experimental use. The monochromator (MONO) has three varied line spacing gratings covering an energy range from 40 to 2000 eV. Argon core-shell excitation spectra shows an energy resolving power of greater than 10^4 at 244 eV. The measured photon flux is 2.3×10^{11} photons/sec/0.1%BW at 244 eV, 3.5 GeV, and 300 mA at the sample.

INTRODUCTION

A high brightness, high photon flux and high coherence of radiation are often generated from undulators, which are scarce and expensive sources. In comparison, beamlines with bending magnet sources are much less expensive and more numerous than insert device sources. The main obstacle to using a bending magnet source is its larger horizontal divergence angle, which can lead to a great aberration and thus reduce the brilliance and energy resolution. Herein, we report an operational soft X-ray bending magnet beamline BL02B at the Shanghai Synchrotron Radiation Facility (SSRF) [1] that generates a beam of relatively high flux and energy resolution. One elliptical cylinder mirror (ECM1) and two ellipsoidal mirrors (EM3 and EM4) are applied to reduce aberration. By using a long pre-focusing elliptical cylinder mirror located at a short distance from the source, three varied-line-spacing gratings (VLSG) and an ellipsoidal mirror of high demagnification ratio, the BL02B beamline can cover the energy range from 40 to 2000 eV with a photon flux of 2.3×10^{11} photons/sec/0.1%BW and energy resolving powers greater than 10^4 at 244 eV. A high energy resolution and high photon flux are essential for ambient pressure photoelectron spectroscopy (APPES) and photon-in/photon-out spectroscopy (PIPOS) to study the

Proceedings of the 13th International Conference on Synchrotron Radiation Instrumentation – SRI2018
AIP Conf. Proc. 2054, 030011-1–030011-6; https://doi.org/10.1063/1.5084574
Published by AIP Publishing. 978-0-7354-1782-3/$30.00

electronic structures of new energy-related environmentally friendly materials. The achieved high performances demonstrate that the bending magnet beamline can be a powerful platform for APPES and PIPOS experiments [2, 3].

A photo and schematic of the optical layout of the BL02B beamline are shown in Fig. 1 and Fig. 2. A four-blade slit (slit 1) is located 8.8 m downstream of the bending magnet source to block the undesirable photons and define the acceptance angle of the beamline. The ECM1 is located 11.1 m after the source. The mirror can focus the beam horizontally onto the exit slits located at 32.4 m [slit 2a for the APPES branch or slit 2b for the PIPOS branch]. To collect a high photon flux, the mirror is manufactured to be 1 m long with a grazing-incident angle of 1.5° and a large acceptance angle of 2 mrad. The BL02B beamline utilizes a variable included angle-varied line spacing plane grating monochromator (VLS-PGM) [4], located 22 m from the source and consisting of one internally water-cooled plane mirror and three varied line spacing gratings. The -1st diffraction order and a C_{ff} (fixed focus constant) value of 0.6 are chosen for the whole energy range. In addition to energy dispersion, the gratings also vertically focus the beam onto the exit slit. The grating with a line spacing of 400 l/mm covers the range of 40 eV to 600 eV while the gratings with 800 and 1100 l/mm cover the range of 200 eV to 2000 eV. The linear groove density can be given by

$$n(x) = n_0(1 + 2n_1x + 3n_2x^2 + 4n_3x^3), \quad (1)$$

where n_0 is the line density at the grating center, x is the coordinate along the grating length and n_1, n_2 and n_3 are the varied-line-spacing parameters used to focus the monochromatic beam on the exit slit, correct the coma aberration, and correct the spherical aberration, respectively. The linear groove density parameters n_1 for the 400 l/mm, 800 l/mm and 1100 l/mm gratings are -12.45×10^{-5} /mm, -12.5×10^{-5} /mm and -12.49×10^{-5} /mm, respectively. The light on the exit slits plane can be observed as a second source for the downstream ellipsoidal mirrors (EM3 and EM4). The entrance and exit arm lengths are 7 m and 2 m for EM3 and 7.8 m and 3.2 m for EM4, respectively. The two mirrors can be used to focus the beam onto the sample positions for APPES (41.4 m) and PIPOS (43.4 m). The main parameters for the beamline are listed in Table 1.

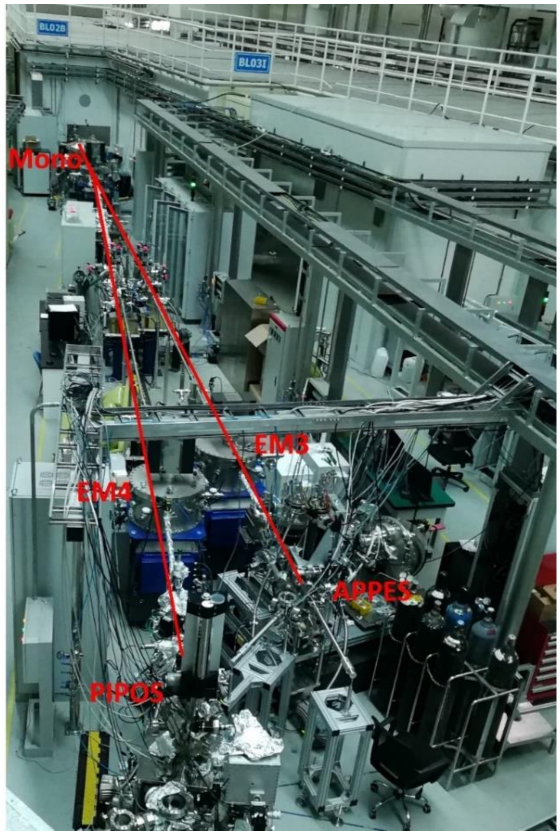

FIGURE 1. The BL02B beamline photo

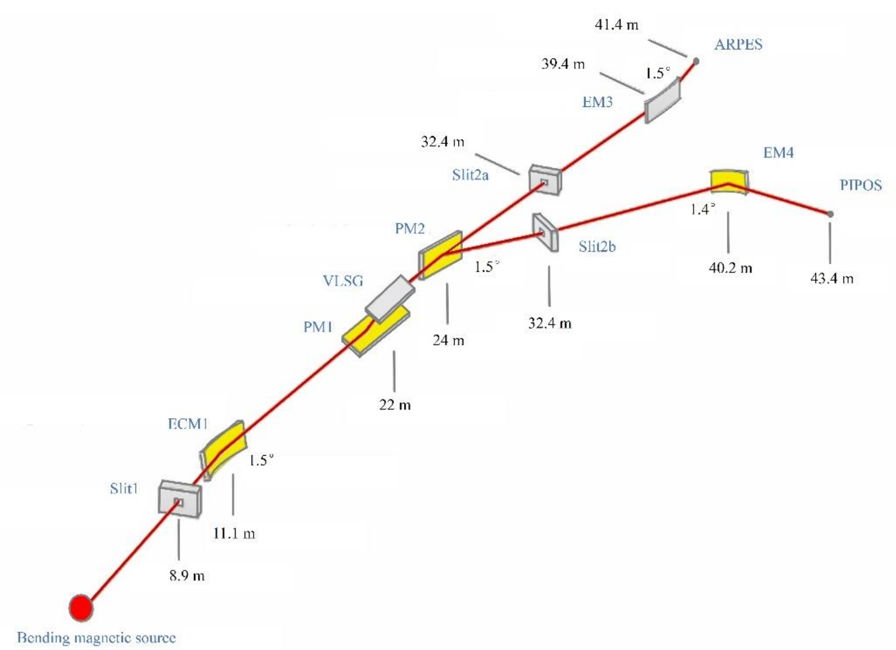

FIGURE 2. The BL02B beamline optical layout

Table 1 Parameters for the beamline optics

Element	Position (m)	Shape	Optical area (L×W) (mm^2)	Deflection /angle (°)	Coating	Slope error (*tan*/*sag*) (μrad)	Roughness (nm)
Slit 1	8.9	--	--	--	--	--	--
ECM1	11.1	Elliptical cylindrical	980 × 40	1.5	Au	0.75/5	0.4
PM1	22	Plane	340 × 30	Variable	Au	0.2/2.5	0.6
VLSG	22	Plane	170 × 30	Variable	Au	0.12/2	0.5
PM2	24	Plane	380 × 30	1.5	Au	0.4/2.3	0.3
Slit 2a	32.4	--	--	--	--	--	--
EM3	39.4	Ellipsoidal	340 × 15	1.5	Au	1/5	0.7
APPES	41.4	--	--	--	--	--	--
Slit 2b	32.4	--	--	--	--	--	--
EM4	40.2	Ellipsoidal	360 × 15	1.4	Au	1/5	0.5
PIPOS	43.4	--	--	--	--	--	--

EXPERIMENTS

An ionization chamber was installed behind the exit slits. The theoretical resolution could be verified by measuring the gas core-shell excitation spectra. The experiments were performed in the chamber with a gas pressure of approximately 10^{-6} Torr. The MONO with an 800 l/mm grating was set to C_{ff} = 0.6, and the exit slit was 15 μm. Figure 3(a) shows the Ar gas core-shell excitation spectra. The electronic transmissions of Ar $L_{2,3}$absorption-edges to Rydberg levels $2p_{3/2}^{-1} \rightarrow nl$ and $2p_{1/2}^{-1} \rightarrow nl$ were clearly detected. The first peak was used to characterize the energy resolution, as shown in Fig. 3(b). The measured spectrum was a Voigt profile, a direct convolution of a Lorentzian natural line width of 112 meV [5] with the Gaussian instrumental width. By Voigt fitting the first peak, we obtained an energy resolution of 21.2 meV. The energy resolving power is greater than 10^4 at 244 eV, which is satisfactory for the APPES and PIPOS experiments.

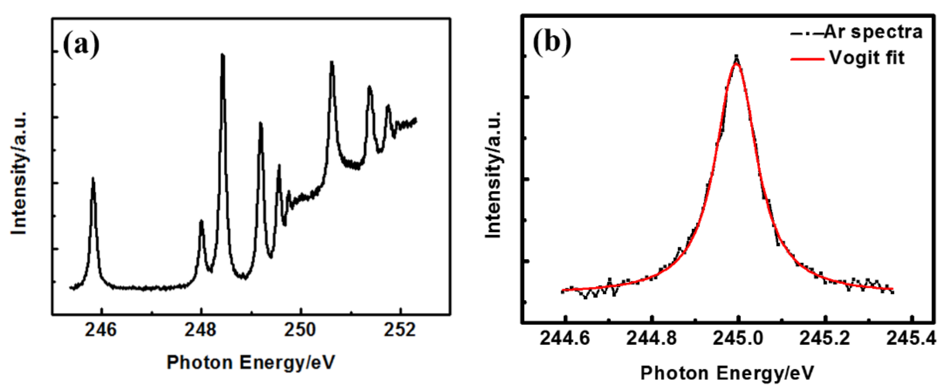

FIGURE 3. (*a*) Excitation spectra for the Ar *L*-edge using the 800 l/mm grating. (*b*) Ar $2p_{3/2} \rightarrow 4s$ transition spectrum. The energy resolution is 21.2 meV with the natural line width of 112 meV.

The APPES endstation contains a fast-access load lock, a sample preparation chamber, an analysis chamber and an energy analyzer. To facilitate fast sample transfers, the load lock chamber is designed to be evacuated to 10^{-7} mbar within an hour. The sample preparation chamber has an ion gun for sputtering and a low-energy electron diffraction (LEED) setup for surface structure characterization. A thin Si_3N_4 membrane is mounted on the analysis chamber to let the X-ray into the sample and separate the ambient-pressure from the beamline. A pre-lens device is used to connect the analysis chamber and the VG Scienta Hipp3 energy analyzer for photoelectron spectroscopy measurements. The ambient pressure in the analysis chamber can vary from UHV to 20 mbar to investigate the working principles of energy materials, electrochemical devices and so on. The ion gauge and capacitance diaphragm gauge are mounted on the analysis chamber to monitor the gas pressure in the range from 10^{-10} mbar to 10^{-4} mbar and from 10^{-4} mbar to 100 mbar, respectively. Additionally, the second differential pumping stage is equipped with a quadrupole mass spectrometer that can monitor the reaction gases.

The PIPOS endstation contains a fast-access load lock, a transfer chamber, a sample preparation chamber and an analysis chamber. The sample preparation chamber has an ion gun for sample cleaning and LEED setup for surface structure characterization. Some separate standard effusion cells are included for the thin-film deposition. The analysis chamber includes a low-temperature sample stage and a high-temperature sample stage, so that the sample temperature can vary from 70 K to 600 K. Additionally, *in situ* charge-discharge experiments for energy materials can be performed under the ultrahigh vacuum (UHV) and ambient pressure conditions. The total electron yield (TEY) and total fluorescence yield (TFY) experiments can be performed with a base pressure of approximately 5×10^{-10} Torr. The TEY and TFY spectra can be normalized to the photon flux recorded using a clean gold mesh, which is installed between the PIPOS branch and the sample. Within a certain approximation, the TEY and TFY spectra are proportional to the number of created core holes. The density of unoccupied states above the Fermi level can be reflected by a combination of the two techniques. Due to the short escape length of electrons, the TEY technique probes the sample surface within a depth of several nanometers. In contrast, the TFY technique has a typical probing depth of several hundreds of nanometers.

We briefly present some results obtained using the APPES and PIPOS endstations. The APPES can provide information for the solid or liquid surfaces in the presence of gases under ambient conditions. The Ag 3d XPS spectrum was measured using the energy analyzer as shown in Fig. 4(a). The pre-lens entrance of the energy analyzer is 0.3 mm from the Ag film. The photon energy and the pass energy for the energy analyzer are aimed as 500 eV and 50 eV, respectively. The kinetic energy obtained from the XPS profile and binding energy for Ag $3d_{5/2}$ obtained from the database are 1639.8 eV and 368.3 eV, respectively. According to the photoelectron spectroscopy principle, the incident photon energy is 2012 eV. The photon flux is much lower at 2000 eV. To increase the signal-to-noise ratio of the measured spectra, the vertical size of the exit slit is enlarged. The energy resolving power decreases to approximately 2000 at 2000 eV. Therefore, the Ag 3d features are broadened into an apparently Gaussian shape. The X-ray absorption spectra of the Ti sample is measured using the TEY technique under the UHV condition at the PIPOS endstation. The fine features of the Ti *L*-edges are clearly observed in Fig. 4(b). In the future, we will use the TFY technique to measure the Ti *L*-edges. The difference in the probing depths between the TEY and TFY techniques can be used to differentiate between the surface and bulk states of Ti samples. The Ti and Ag spectra demonstrate that the BL02B beamline can perform APPES and PIPOS experiments.

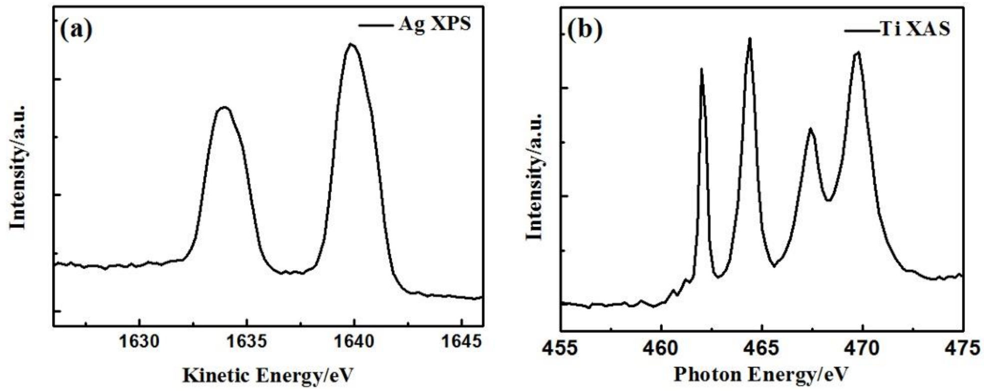

FIGURE 4.(*a*) Ag3d XPS for the Ag film at the APPES endstation. (*b*) Soft XAS for the Ti sample at the PIPOS endstation.

CONCLUSION

The BL02B bending magnet beamline at the SSRF is dedicated to high energy resolution and high photon flux experiments and is operational now. Due to the high performance within a wide energy range from 40 eV to 2000 eV, the BL02B beamline can be utilized to perform novel APPES and PIPOS experiments.

ACKNOWLEDGMENTS

This work was supported by the National Major Scientific Instruments and Equipment Development of NSFC (11227902) and the National Natural Science Foundation of China (No. 11575284, 11475251, and 11705272).

REFERENCES

1. Z. Guo, X. Y.Meng, Y. Wang, H. G. Liu, X. Z. Zhang, Z. L. Li, L. Xue and R. Z, Tai.J. Synchrotron Rad.**24**, 877-885(2017).
2. M. Salmeron and R.Schlögl,Surf. Sci. Rep.**63**, 169-199(2008).
3. F.Himpsel, Physica Status Solidi(b)**248**, 292-298 (2011).
4. Y. F. Hu, L.Zuin, G.Wright, R.Igarashi, M.McKibben, T.Wilson, S. Y.Chen, T.Johnson, D.Maxwell, B. W.Yates, T. K.Sham andR.Reininger,Rev. Sci. Instrum.**78**, 083109 (2007).
5. V. N.Strocov, T. Schmitt, U. Flechsig, T. Schmidt, A. Imhof, Q. Chen, J. Raabe, R. Betemps, D. Zimoch, J. Krempasky, X. Wang, M. Grioni, A. Piazzalunga, andL.Patthey, J. Synchrotron Rad.**17**, 631-643(2010).